Deuterium NMR of Val[1]···(2-^{2}H)Ala[3]···Gramicidin A in Oriented DMPC Bilayers†

Andrew W. Hing,*,‡ Steven P. Adams,§ David F. Silbert,∥ and Richard E. Norberg‡

Department of Physics, Washington University, St. Louis, Missouri 63130, Department of Biochemistry and Molecular Biophysics, Washington University, St. Louis, Missouri 63110, and Central Research Laboratory, Monsanto Company, Chesterfield, Missouri 63198

Received June 27, 1989; Revised Manuscript Received December 8, 1989

ABSTRACT: Deuterium NMR is used to study the selectively labeled Val[1]···(2-^{2}H)Ala[3]···gramicidin A molecule to investigate the structure and dynamics of the C_α–^{2}H bond in the Ala[3] residue of gramicidin. Val[1]···(2-^{2}H)Ala[3]···gramicidin A is synthesized, purified, and characterized and then incorporated into oriented bilayers of dimyristoylphosphatidylcholine sandwiched between glass coverslips. Phosphorus NMR line shapes obtained from this sample are consistent with the presence of the bilayer phase and indicate that no nonbilayer phases are present in significant amounts. Deuterium NMR line shapes obtained from this sample indicate that the motional axis of the gramicidin Ala[3] residue is parallel to the coverslip normal, that the distribution of motional axis orientations has a width of 2°, and that only one major conformational and dynamical state of the Ala[3] C_α–^{2}H bond is observed on the NMR time scale. Furthermore, the Ala[3] C_α–^{2}H bond angle relative to the motional axis is 19–20° if fast axial rotation is assumed to be the only motion present but is ≤19–20° in the absence of such an assumption. This result indicates that various double-stranded, helical dimer models are very unlikely to represent the structure of gramicidin in the sample studied but that the single-stranded, $\beta^{6.3}$ helical dimer models are consistent with the experimental data. However, a definitive distinction between the left-handed, single-stranded, $\beta^{6.3}$ helical dimer model and the right-handed, single-stranded, $\beta^{6.3}$ helical dimer model cannot be made on the basis of the experimental data obtained in this study.

Natural gramicidin is a linear peptide produced by the bacteria *Bacillus brevis* (Hotchkiss & Dubos, 1941) and is actually a mixture of components designated gramicidin A, gramicidin B, and gramicidin C (Gregory & Craig, 1948); furthermore, each of these components comes in two different forms. Thus, the natural mixture is composed of six different gramicidins with the primary structures (Sarges & Witkop, 1965a–c)

HCO-L-Val[1]-Gly[2]-L-Ala[3]-D-Leu[4]-L-Ala[5]-D-Val[6]-L-Val[7]-D-Val[8]-L-Trp[9]-D-Leu[10]-L-AAA[11]-D-Leu[12]-L-Trp[13]-D-Leu[14]-L-Trp[15]-NHCH$_2$CH$_2$OH

HCO-L-Ile[1]-Gly[2]-L-Ala[3]-D-Leu[4]-L-Ala[5]-D-Val[6]-L-Val[7]-D-Val[8]-L-Trp[9]-D-Leu[10]-L-AAA[11]-D-Leu[12]-L-Trp[13]-D-Leu[14]-L-Trp[15]-NHCH$_2$CH$_2$OH

where AAA denotes Trp for gramicidin A, Phe for gramicidin B, and Tyr for gramicidin C.

One of the most important properties of gramicidin is its ability to form ion channels in model membranes (Hladky & Haydon, 1970, 1972). Ion channels in cell membranes are extremely important for cellular functions such as controlling the internal environment, maintaining a membrane potential, and, in nerve cells, propagating an action potential. It is hoped that study of a model ion channel such as gramicidin will lead to general insights about how ion channels work.

An understanding of the functional aspects of the gramicidin channel requires, however, a knowledge of the structural aspects of the channel. Specifically, the three-dimensional structure of the main ion-transporting channel of gramicidin in membranes is postulated to be a dimer composed of two left-handed, single-stranded, $\beta^{6.3}$ helices with 6.3 amino acids per turn (Urry, 1971; Urry et al., 1971). A fair amount of experimental evidence exists for the postulated $\beta^{6.3}$ helical structure of the transmembrane gramicidin channel (Weinstein et al., 1979, 1980, 1985; Urry et al., 1971, 1982a,b, 1983a; Wallace et al., 1981), but this experimental evidence provides only indirect support for the postulated $\beta^{6.3}$ helical structure. This support is indirect in the sense that the structure of the gramicidin channel in a membrane is not determined to atomic resolution. Consequently, more recent structural studies of the gramicidin channel obtain information by solid-state NMR which can directly observe the structure and dynamics of gramicidin at atomic resolution in a membrane. These studies have used the ^{13}C chemical shift anisotropy (Cornell et al., 1988), the ^{15}N chemical shift anisotropy (Nicholson et al., 1987; Fields et al., 1988), the ^{13}C–^{13}C magnetic dipolar interaction (Cornell et al., 1988), and the ^{2}H electric quadrupolar interaction (Datema et al., 1986; Macdonald & Seelig, 1988) to monitor the conformation and dynamics of gramicidin in phospholipid bilayers. One study has also examined gramicidin in a lyotropic, nematic liquid-crystalline phase (Davis, 1988). From these studies, a clearer picture of the structure and dynamics of gramicidin in a membrane is beginning to emerge.

In this paper, deuterium NMR is used to investigate the structure and dynamics of a selectively deuterated gramicidin incorporated into oriented phospholipid bilayers. The use of deuterium NMR to study structure and dynamics is advantageous because the relatively large quadrupolar interaction of the deuterium nucleus in a C–^{2}H bond provides a wide dynamic range over which measurements can take place and because the near axial symmetry of the C–^{2}H quadrupolar

† This work was supported in part by NIH Grants GMO7200, GM30244, and GM38540, ACS Grant BC198, the Department of Physics of Washington University, and the Central Research Laboratories of Monsanto Co.

* Address correspondence to this author at the Department of Physics, Box 1105, Washington University, St. Louis, MO 63130.

‡ Department of Physics, Washington University.

§ Monsanto Co.

∥ Department of Biochemistry and Molecular Biophysics, Washington University.

0006-2960/90/0429-4144$02.50/0

interaction permits conclusions about the quadrupolar interaction to be related directly to the molecular frame. The selective labeling of one atom allows all resonance lines to be assigned to a single, specific site. This knowledge is required to fully interpret the NMR spectra. The deuterated gramicidin is incorporated into oriented DMPC[1] bilayers because this permits the anisotropy of the structure and dynamics to be studied; this information is lost in a randomly oriented sample such as multilamellar vesicles. Also, phosphorus NMR spectra of the phosphocholine headgroup of DMPC are obtained because this provides a convenient way to monitor the behavior of the surrounding lipid matrix.

The selectively deuterated gramicidin studied in this paper is the Val[1] form of gramicidin A in which a deuteron replaces the proton normally bonded to the α carbon of Ala[3]. The structure and dynamics of this backbone α carbon in a bilayer are monitored via the quadrupolar interaction of the C_α–^{2}H bond. Specifically, deuterium line shapes are obtained of the selectively deuterated gramicidin. The deuterium resonance lines are analyzed in terms of quadrupolar splitting, line width, and number. This allows conclusions to be drawn about the conformation, the distribution of orientations about some mean orientation, and the number of conformational and dynamical states of the Ala[3] C_α–^{2}H bond on the NMR time scale. A similar analysis of phosphorus line shapes of the surrounding lipid matrix yields information about the molecular orientation of DMPC. The conformation and dynamics of the Ala[3] C_α–^{2}H bond of gramicidin can then be interpreted in terms of the behavior of the surrounding lipid matrix. This interpretation can ultimately be related to theoretical models of channel structure.

Experimental Procedures

Peptide Synthesis

Synthesis. Selective deuteration of the α carbon of Ala[3] in gramicidin is accomplished by first incorporating the specifically deuterated amino acid (2-^{2}H) alanine into gramicidin by the solid-phase method (Merrifield, 1963). The procedure for synthesizing gramicidin by this method essentially follows that developed by Gross and co-workers (Fontana & Gross, 1972; Noda & Gross, 1972) and Prasad et al. (Prasad et al., 1982; Urry et al., 1982b) with some slight modifications (Hing, 1990).

Purification. Purification of the crude peptide is achieved by countercurrent chromatography performed on a coil planet centrifuge (P. C. Inc.) (Ito, 1986) and by preparative thin-layer chromatography. The procedure for purifying gramicidin by countercurrent chromatography is outlined by Ito et al. (1982), and the use of preparative TLC in the purification process of crude gramicidin is demonstrated by Prasad et al. (1982). The exact details of the procedure followed in the purification process are described elsewhere (Hing, 1990).

Characterization. The purified Val[1]···(2-^{2}H)Ala[3]···gramicidin A is characterized by HPLC, TLC, ^{13}C NMR, mass spectrometry, and amino acid analysis.

Sample Preparation

The incorporation of Val[1]···(2-^{2}H)Ala[3]···gramicidin A into oriented DMPC bilayers is accomplished by the procedure outlined by Seelig et al. (1985) and Nicholson et al. (1987) with some modifications. The procedure basically involves mixing the lipid and peptide, depositing the mixture onto glass coverslips, and hydrating and aligning the lipid–peptide deposits.

The mixing of DMPC and gramicidin is accomplished in a solution of methanol. Specifically, DMPC (Avanti Polar Lipids, Inc.) and synthetic Val[1]···(2-^{2}H)Ala[3]···gramicidin A are mixed together in a molar ratio of 10:1 lipid/peptide in a solution of methanol at a concentration of 9.20 mg of lipid–peptide/mL of methanol.

Deposition of the DMPC–gramicidin mixture onto glass coverslips is accomplished by division of the stock solution into smaller volumes and deposition of the lipid–peptide mixture in each volume onto a separate coverslip surface. Moreover, both sides of a coverslip are used for deposition. The deposition of each lipid–peptide mixture onto a coverslip surface involves the following steps: (1) withdrawal of a volume of 1 mL from the stock solution; (2) evaporation of the methanol from this aliquot by a gentle stream of nitrogen; (3) dissolution of the residue remaining in 29 μL of 86.2% methanol (Burdick and Jackson) in deuterium-depleted water (Isotec); (4) deposition of the resulting solution onto the surface of a 7.5 mm × 22 mm coverslip (Corning Cover Glasses No. 1) that has been prewashed successively in distilled, deionized water, methanol, and chloroform; (5) undisturbed evaporation under ambient conditions of most of the solvent from the deposit; (6) drying of the deposit under vacuum over phosphorus pentoxide for 2 days. The resulting coverslips, most of which possess deposits on both sides, are then stacked one on top of the other with spacers located between coverslips. A total of 63 ± 3 mg of Val[1]···(2-^{2}H)Ala[3]···gramicidin A is contained in this stack of coverslips.

Hydration and alignment of the individual DMPC–gramicidin layers is accomplished by heating of the sample in an atmosphere saturated with water vapor in a magnetic field. The stack of coverslips containing the lipid–peptide mixture is placed inside a square glass tube whose inner dimensions are 8 mm × 8 mm. A water reservoir inside the square glass tube is filled with enough deuterium-depleted water (Isotec) to keep the atmosphere inside the tube saturated with water vapor. The sample tube is then sealed and placed inside a 4.7-T magnetic field with the normal to the glass coverslips oriented at 90° with respect to the magnetic field direction (β = 90°). The sample is heated in this configuration with a stream of thermally regulated air. Heating of the sample is alternated with some manual compression of the sample stack. The sample is heated for a total of 21 h at 44 °C and 27 h at 49 °C.

NMR Probe

The NMR probe used to obtain solid-state phosphorus and deuterium spectra is constructed to have electrical, mechanical, and thermal capabilities that facilitate the observation of phosphorus and deuterium nuclei in oriented samples. Electrically, the probe circuit can handle high power and can be doubly tuned to 200 MHz (^{1}H) and one other frequency, usually 81 MHz (^{31}P) or 31 MHz (^{2}H). The doubly tuned circuit thus allows proton-decoupled spectra of phosphorus or deuterium to be observed. Mechanically, a goniometer built into the probe controls sample orientation with respect to the magnetic field (Pines et al., 1974). To control the temperature of the sample, a thermostating gas (air above room temperature and nitrogen below room temperature) is pumped into the sample chamber of the probe. A Bruker B-VT 1000 unit provides temperature regulation of the gas above and below

[1] Abbreviations: DMPC, dimyristoylphosphatidylcholine; GA, gramicidin A; GB, gramicidin B; GC, gramicidin C; HPLC, high-performance liquid chromatography; TLC, thin-layer chromatography; RTD, resistance temperature detector or resistance thermometry device; T_2, spin–spin relaxation time; t_R, time between repetitions of pulse sequence; τ, time between pulses of quadrupole echo sequence.

room temperature. The temperature readings of the Bruker unit, though, are calibrated with a platinum RTD (Yellow Springs Instrument PT 139) to provide a more accurate measure of the temperature at the sample.

NMR Data Acquisition

Orientation. The angle between the normal to the glass coverslips and the direction of the magnetic field is designated β, and the effect of macroscopic sample orientation on the NMR spectrum is studied by variation of the angle β. In particular, NMR spectra are obtained at two different orientations: $\beta = 0°$ and $\beta = 90°$. Before each NMR run, the sample is equilibrated in the magnetic field at $T = 44$ °C and $\beta = 90°$ for at least a few hours.

Temperature. The effect of temperature on the resultant NMR spectra is studied by variation of the temperature T in 10 °C increments. At each temperature, the sample is equilibrated for 1 h before NMR data are acquired.

Phosphorus NMR. Phosphorus NMR spectra are acquired with a Bruker CXP200 spectrometer operating at 81 MHz. A real spectrum is 2048 points in size and is acquired with a spectral width of 15.152 kHz, thereby yielding a digital resolution of 7.398 Hz/point. A single 3.86-μs pulse is used to acquire the phosphorus spectra with a recycle delay of $t_R = 10$ s. The single pulse is phase cycled to minimize instrumental inaccuracies (Hoult & Richards, 1975; Stejskal & Schaefer, 1974). Also, phosphorus spectra are acquired in the presence of a proton-decoupling field whose strength is estimated to be approximately 20 kHz. The duty cycle of the proton-decoupling field is set to 0.1% to minimize radio frequency heating effects. Phosphorus spectra are plotted with a line broadening of 20 Hz and are referenced to external 85% phosphoric acid.

Deuterium NMR. Deuterium NMR spectra are acquired with a Bruker CXP200 spectrometer operating at 31 MHz. A real spectrum is 2048 points in size and is acquired with a spectral width of 1.6667 MHz, thereby yielding a digital resolution of 813.8 Hz/point. Because the deuterium 90° pulse width is 5 μs, a second order, composite quadrupole echo sequence (Levitt et al., 1984) is used to acquire all deuterium spectra. In this sequence, a composite 90° pulse consists of $(90°_{+x})(180°_{-x})(90°_{+x})(135°_{-x})(45°_{+x})$. Data are acquired with a fully phase cycled (Griffin, 1981) version of this sequence. For spectra acquired with proton decoupling, the strength of the proton-decoupling field is estimated to be 30 kHz, and the duty cycle of the proton-decoupling field is kept below 0.2% to minimize radio frequency heating effects. Deuterium spectra of membranes are acquired with a recycle delay of $t_R = 0.5$ s, zero filled to twice the original spectral size, plotted without added line broadening, and referenced to external ^2H_2O.

RESULTS

Phosphorus NMR

Phosphorus NMR spectra of the DMPC–gramicidin sample are shown in Figure 1 as a function of macroscopic sample orientation and temperature. Parts a–e of Figure 1 correspond to a sample oriented at $\beta = 0°$, while parts f–j of Figure 1 correspond to a sample oriented at $\beta = 90°$. These spectra are obtained at temperatures ranging from $T = 44$ °C to $T = 4$ °C. The phase transition between the liquid-crystalline and gel states has been shown for similar mixtures of phosphatidylcholine and gramicidin to be a broadened transition which is approximately 9 °C in breadth and which occurs within a few degrees of the phase transition temperature of the pure lipid (Chapman et al., 1974, 1977; Nicholson et al., 1987). Consequently, the temperatures at which the spectra of Figure 1 are obtained encompass the phase transition temperature.

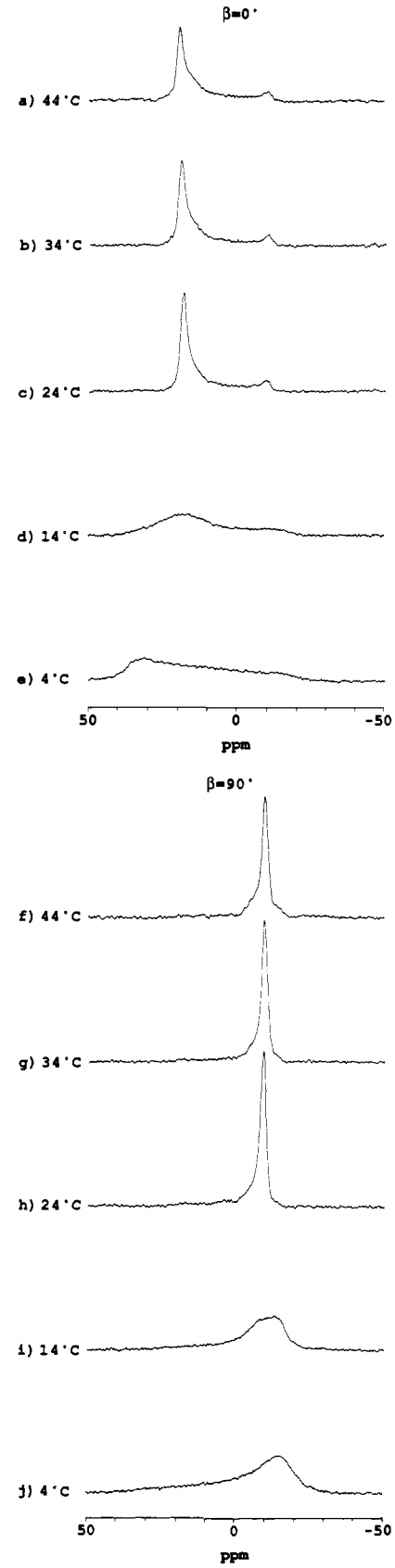

FIGURE 1: Orientation and temperature dependence of the ^{31}P NMR spectrum of DMPC bilayers containing Val^1···(2-^{2}H)Ala^3···gramicidin A. All spectra are acquired with $t_R = 10.0$ s, 12 scans, and ^1H decoupling.

Table I: ^{31}P NMR Chemical Shift Anisotropy and Line Widths of Oriented DMPC Bilayers Containing Val[1]···(2-^{2}H)Ala[3]···Gramicidin A as a Function of Temperature and Sample Orientation

	$\beta = 0°$		$\beta = 90°$		
T (°C)	ν_{CSA}[a] (ppm)	fwhm[b] (ppm)	ν_{CSA} (ppm)	fwhm (ppm)	$\Delta\sigma$ (ppm)
44	19.6	2.5	−9.3	2.1	28.9
34	19.3	2.8	−9.3	2.0	28.6
24	18.2	2.6	−8.8	2.2	27.0
14	~20	~20	~−10	~15	~30
4	~30	~25	~−15	~15	~45

[a] ν_{CSA} is referenced to external 85% phosphoric acid. [b] fwhm is the full width of the resonance line at half-intensity.

Molecular Orientation. An analysis of the orientation dependence of the resonance frequency of the main phosphorus resonance line yields some information about the molecular orientation of the phosphocholine headgroup. The resonance frequency of the main peak in the spectra of Figure 1 is listed in Table I and is referenced to external 85% phosphoric acid. Table I shows that the resonance frequency of the main peak varies with sample orientation in such a way that the frequency measured at $\beta = 0°$ is approximately twice the magnitude of the frequency measured at $\beta = 90°$. This result indicates that the DMPC headgroup rotates rapidly about an axis close to parallel to the normal to the glass coverslips. In particular, when the ^{31}P chemical shift tensor of the phosphocholine headgroup, which has three unique tensor elements σ_{11}, σ_{22}, and σ_{33} in the absence of motion, is motionally averaged to an axially symmetric tensor with elements $\sigma_\parallel$ and $\sigma_\perp$ by rapid rotation about an axis, the resonance frequency ν_{CSA} of the phosphorus nucleus in the headgroup obeys the equation (Seelig, 1978)

$$\nu_{CSA} = -(2/3)\Delta\sigma(3\cos^2\beta' - 1)/2 \quad (1)$$

where ν_{CSA}, $\sigma_\parallel$, and $\sigma_\perp$ are measured in parts per million relative to the resonance frequency that results from fast isotropic motion, $\nu_{CSA}(\beta' = 0°) = -\sigma_\parallel$, $\nu_{CSA}(\beta' = 90°) = -\sigma_\perp$, $\Delta\sigma = \sigma_\parallel - \sigma_\perp$, and β' is the angle between the axis of motional averaging and the direction of the magnetic field. Although the values of ν_{CSA} listed in Table I are referenced to external 85% phosphoric acid, a spectrum of a similar mixture of DMPC and gramicidin in vesicle form indicates that fast isotropic motion of the DMPC molecules results in a resonance frequency which is within 1 ppm of the resonance frequency of 85% phosphoric acid. The values of ν_{CSA} for $\beta = 0°$ and $\beta = 90°$ measured from the spectra of Figure 1 and tabulated in Table I therefore obey eq 1 if the axis of motional averaging is parallel to the normal to the glass coverslips, in other words if $\beta' = \beta$.

Distribution of Orientations. An analysis of the line width of the main phosphorus resonance lines yields information about the distribution of phosphocholine motional axis orientations about some mean orientation. In Figure 1, the line width and symmetry of the main resonance peak show a dependence on macroscopic sample orientation at all temperatures. The line width of the main resonance peak in the spectra of Figure 1 is listed in Table I and is generally larger for the $\beta = 0°$ sample orientation than for the $\beta = 90°$ sample orientation at all temperatures. In terms of symmetry, the line shape in the spectra of Figure 1 exhibits an orientation-dependent asymmetry at all temperatures which is apparent as an increased intensity at the base of the resonance line on the low-frequency side for the $\beta = 0°$ sample orientation and on the high-frequency side for the $\beta = 90°$ sample orientation. Equation 1 shows that the general features of this dependence of line width and symmetry on macroscopic sample orientation can be explained by inhomogeneous line broadening arising from a distribution of phosphocholine motional axis orientations in which most motional axes are aligned parallel to the coverslip normal. Moreover, from eq 1, the line width of the resonance, and an assumed fixed, homogeneous line-width contribution, an estimate can be made of the width of the distribution of β' angles about $\beta' = 0°$ for the $\beta = 0°$ sample orientation. This width is estimated to be ~7° at temperatures near and above the phase transition temperature; at temperatures below the phase transition temperature, intermolecular ^{31}P–^{1}H dipolar interactions give rise to a large amount of homogeneous line broadening (Niederberger & Seelig, 1976; Hemminga & Cullis, 1982) which prevents an accurate estimate of the β' distributional width from being made. However, while inhomogeneous line broadening arising from a distribution of motional axis orientations can explain to a large extent the orientation-dependent features of the observed phosphorus resonance lines, anisotropic T_2 relaxation may also be partly responsible for the observed results (Rajan et al., 1981).

Number of Phases. The number of different types of phosphorus resonance lines in the spectra of Figure 1 yields information about the number of different types of lipid phases present. The spectra of Figure 1 obtained near and above the phase transition temperature show that most of the phosphorus signal is concentrated in one main resonance peak; this indicates that most of the DMPC headgroups in the sample are rapidly rotating about the coverslip normal at temperatures near and above the phase transition temperature. No signals are present in these spectra which could be interpreted to indicate the presence of the inverted hexagonal phase or phases consisting of DMPC molecules undergoing fast isotropic motion.

However, the line shapes of Figure 1 obtained near and above the phase transition temperature do show that a small amount of the total ^{31}P signal is present as a line shape which is characteristic of randomly oriented motional axes. When the sample is oriented at $\beta = 0°$ (Figure 1a–c), the low-frequency peak of the line shape characteristic of randomly oriented motional axes is evident. When the sample is oriented at $\beta = 90°$ (Figure 1f–h), the high-frequency shoulder of the line shape characteristic of randomly oriented motional axes is just barely visible. However, parts a–c and f–h of Figure 1 also show that the line shape of the randomly oriented component does not possess enough intensity to significantly affect the characteristics of the resonance line arising from the oriented component.

Below the phase transition temperature, no firm conclusions can be reached about the amount of other components present because of the broadened nature of the line shape.

Deuterium NMR

Powder Spectrum. The deuterium NMR spectrum of the powder form of pure Val[1]···(2-^{2}H)Ala[3]···gramicidin A is shown in Figure 2b. The large frequency difference between the main peaks of the line shape indicates that the C_α–^{2}H bond in the Ala[3] residue is nearly immobile on the ^{2}H NMR time scale. Furthermore, the overall line shape indicates that a randomly oriented, nearly axially symmetric, electric field gradient tensor is present. For comparison, Figure 2a shows a spectrum of deuterated polyethylene (MSD Isotopes) acquired with the same composite quadrupole echo sequence.

Effect of Interpulse Delay on Membrane Spectra. Deuterium NMR spectra of the DMPC–gramicidin sample are shown in Figure 3 as a function of macroscopic sample orientation and temperature. Parts a–e of Figure 3 correspond

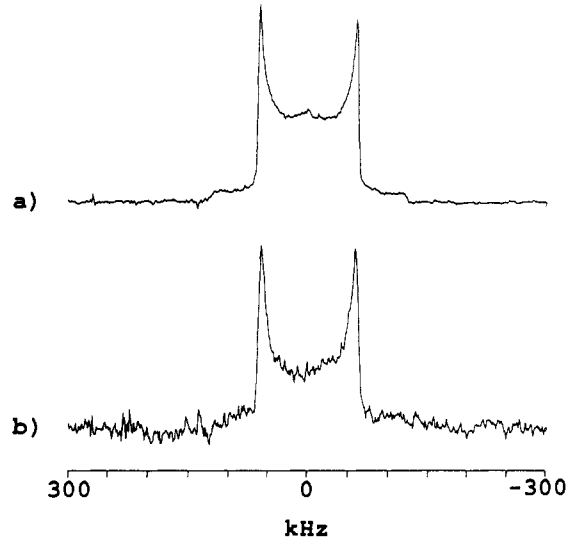

FIGURE 2: ^{2}H NMR spectra of the powder form of (a) perdeuterated polyethylene (230 mg) acquired with 120 scans and (b) Val^1···(2-^{2}H)Ala^3···gramicidin A (175 mg) acquired with 165 696 scans. The spectra are obtained at T = 27 °C with τ = 60 μs, t_R = 2.0 s, and without ^{1}H decoupling. These spectra are plotted with 1 kHz of line broadening.

Table II: ^{2}H NMR Quadrupolar Splittings and Line Widths of Val^1···(2-^{2}H)Ala^3···Gramicidin A in Oriented DMPC Bilayers as a Function of Temperature and Sample Orientation for τ = 200 μs

	β = 0°		β = 90°	
T (°C)	$\lvert\Delta\nu_Q\rvert$[a] (Hz)	fwhm[b] (Hz)	$\lvert\Delta\nu_Q\rvert$ (Hz)	fwhm (Hz)
44	205 900	1000	103 000	800
34	207 500	900	103 800	900
24	N/O[c]	N/O	N/O	N/O
14	N/O	N/O	120 200	3000
4	N/O	N/O	118 800	3700

[a] $\lvert\Delta\nu_Q\rvert$ is measured from the center of one resonance line to the center of the other resonance line and is resolved to 1600 Hz. [b] fwhm is the full width of the resonance line at half-intensity. [c] N/O means that the data could not be observed in the spectrum.

Table III: ^{2}H NMR Quadrupolar Splittings and Line Widths of Val^1···(2-^{2}H)Ala^3···Gramicidin A in Oriented DMPC Bilayers as a Function of Temperature and Sample Orientation for τ = 60 μs

	β = 0°		β = 90°	
T (°C)	$\lvert\Delta\nu_Q\rvert$[a] (Hz)	fwhm[b] (Hz)	$\lvert\Delta\nu_Q\rvert$ (Hz)	fwhm (Hz)
44	205 900	1000	103 000	800
34	N/A[c]	N/A	103 800	1100
24	N/O[d]	N/O	105 800	2100
14	N/A	N/A	N/A	N/A
4	N/O	N/O	118 800	2800

[a] $\lvert\Delta\nu_Q\rvert$ is measured from the center of one resonance line to the center of the other resonance line and is resolved to 1600 Hz. [b] fwhm is the full width of the resonance line at half-intensity. [c] N/A means that the spectrum was not acquired. [d] N/O means that the data could not be observed in the spectrum.

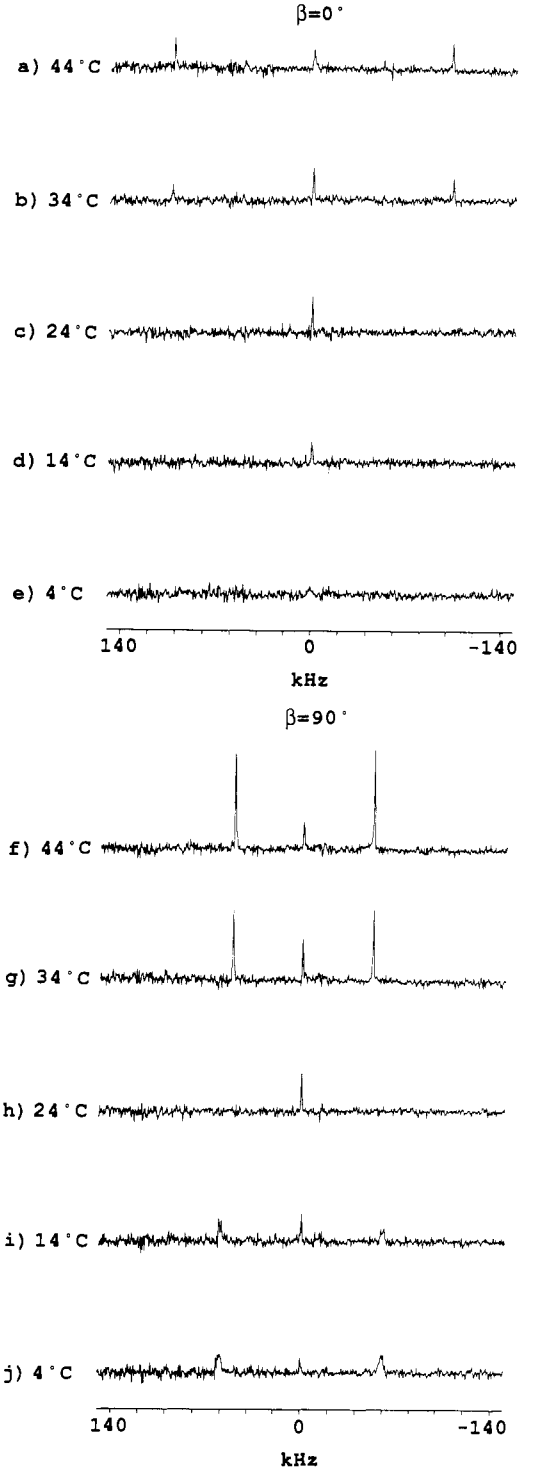

FIGURE 3: Orientation and temperature dependence of the ^{2}H NMR spectrum of Val^1···(2-^{2}H)Ala^3···gramicidin A in DMPC bilayers. All spectra are acquired with τ = 200 μs, t_R = 0.5 s, 80 000 scans, and ^{1}H decoupling.

to a sample oriented at β = 0°; while parts f–j of Figure 3 correspond to a sample oriented at β = 90°. These spectra are acquired at the same temperatures as those used in the acquisition of the ^{31}P NMR spectra shown in Figure 1. The quadrupolar splittings and line widths of the main deuterium resonance lines of Figure 3 are listed in Table II. Because these deuterium spectra are acquired with a quadrupole echo technique, the delay between pulses may allow T_2 relaxation to distort the resulting spectra (Spiess & Sillescu, 1981; Beshah et al., 1987; Vega & Luz, 1987). To determine whether the spectra of Figure 3 have been significantly distorted because of anisotropic T_2 relaxation, some spectra are acquired with a shorter time delay of τ = 60 μs between pulses. Figure 4 shows a comparison of two spectra acquired at T = 44 °C and β = 90° with different values for the time delay between pulses (τ = 60 and 200 μs). Similar results are obtained at other temperatures for spectra acquired with different τ values. The quadrupolar splittings and line widths of the main deuterium resonance lines of Figure 4a and other spectra acquired with τ = 60 μs are listed in Table III. These spectra demonstrate that although some intensity is lost from the spectra obtained with the longer τ value, the general features of the deuterium resonance lines that can be observed with τ = 200 μs are not

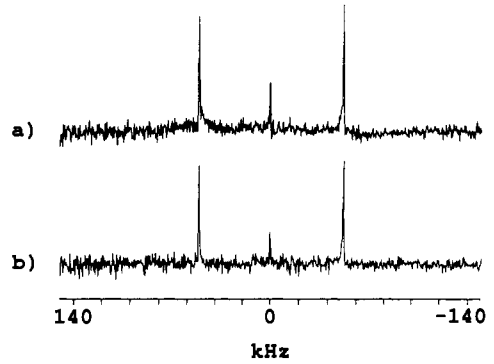

FIGURE 4: Effect of interpulse delay on the ^{2}H NMR spectrum of Val[1]···(2-^{2}H)Ala[3]···gramicidin A in oriented DMPC bilayers above the phase transition temperature. The spectra are acquired with (a) τ = 60 μs and (b) τ = 200 μs. Both spectra are obtained at T = 44 °C and β = 90° with t_R = 0.5 s, 40000 scans, and ^{1}H decoupling.

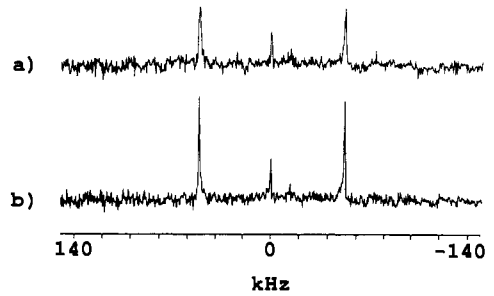

FIGURE 5: Effect of ^{1}H decoupling on the ^{2}H NMR spectrum of Val[1]···(2-^{2}H)Ala[3]···gramicidin A in oriented DMPC bilayers above the phase transition temperature. The spectra are acquired (a) without ^{1}H decoupling and (b) with ^{1}H decoupling. Both spectra are obtained at T = 34 °C and β = 90° with τ = 60 μs, t_R = 0.5 s, and 40000 scans.

significantly altered when τ is decreased to 60 μs.

Effect of ^2H–^1H Dipolar Interactions on Membrane Spectra. The importance of the ^{2}H–^{1}H dipolar interaction as a potential source of anisotropic T_2 relaxation or T_2 relaxation in general is most clearly demonstrated by acquiring spectra with and without proton decoupling. The effect of proton decoupling on spectra acquired above the phase transition temperature is demonstrated in Figure 5. The resonance lines in Figure 5a are acquired at T = 34 °C and β = 90° without proton decoupling, and they possess a full width at half-intensity of 1900 Hz; the resonance lines in Figure 5b are acquired at T = 34 °C and β = 90° with proton decoupling, and they possess a full width at half-intensity of 1100 Hz. Thus, ^{2}H–^{1}H dipolar broadening can increase the line width by approximately 75% in the liquid-crystalline phase of this oriented DMPC–gramicidin system. Similar but stronger effects of ^{2}H–^{1}H dipolar interactions on line shape are observed below the phase transition temperature. Because the ^{2}H–^{1}H dipolar interaction produces a measurable effect on the deuterium line shape of the deuterated gramicidin in these oriented DMPC bilayers, deuterium spectra of these membrane samples are acquired with proton decoupling.

Intensity Changes in Membrane Spectra. Interpretation of the intensity changes observed in the deuterium spectra yields some information about the dynamics of the Ala[3] C_α–^{2}H bond. In Figure 3, as the temperature decreases from above the phase transition temperature, the intensity of the deuterium resonance lines decreases until no signal can be observed at a temperature near the phase transition temperature. As the temperature decreases below the phase transition temperature, ^{2}H NMR signals become observable again, at least for the β = 90° sample orientation. More information about the behavior of the ^{2}H NMR signal near the phase transition temperature is provided by Table III, which shows that ^{2}H NMR resonance lines do appear in a spectrum acquired at T = 24 °C when τ = 60 μs, at least for the β = 90° sample orientation. These results can be explained by the temperature-dependent T_2 relaxation mechanism proposed for an exchange-deuterated synthetic peptide incorporated into DPPC bilayers (Pauls et al., 1985) and for exchange-deuterated gramicidin incorporated into DPPC bilayers (Datema et al., 1986). Studies of these systems show that a minimum in the value of T_2 occurs at the phase transition temperature of the lipid matrix; this minimum in the value of T_2 is interpreted to result from motion intermediate between fast axial rotation ($\gg 10^5$ Hz) and slow motion ($\ll 10^5$ Hz) (Pauls et al., 1985; Datema et al., 1986). Consequently, the observed intensity decrease near the phase transition temperature can be explained as resulting from most deuterium nuclei possessing a value of T_2 too short to be observed with the fixed τ values used in this study.

At all temperatures, the intensities of the main deuterium resonance lines for the β = 0° sample orientation are decreased compared to the intensities of the main deuterium resonance lines for the β = 90° sample orientation. Anisotropic relaxation effects or possibly instrumental limitations may be responsible for this observed intensity decrease.

Molecular Conformation. The orientation dependence and the value of the quadrupolar splitting yield information about the conformation and dynamics of the Ala[3] C_α–^{2}H bond. In particular, rapid rotation of the gramicidin molecule about an axis in the liquid-crystalline phase of the lipid matrix motionally averages the electric field gradient tensor of the C–^{2}H bond in such a way that the quadrupolar splitting $\Delta\nu_Q$ of the deuterium nucleus obeys the equation (Seelig, 1977)

$$\Delta\nu_Q = (3/2)(e^2qQ/h)\langle(3\cos^2\theta - 1)/2\rangle(3\cos^2\beta' - 1)/2 \quad (2)$$

This equation assumes that the electric field gradient tensor is axially symmetric, an assumption justified by the fact that the asymmetry parameter η for C–^{2}H bonds is generally small enough to be negligible ($\eta \sim 0.05$) (Seelig, 1977). The angle θ is the angle between the axis of motional averaging and the unique axis of the molecularly fixed, principal axis system of the electric field gradient tensor; but since the unique axis of the molecularly fixed, principal axis system of the electric field gradient tensor is generally the same as the C–^{2}H bond vector, the angle θ also represents the angle between the motional axis and the C–^{2}H bond vector. The term e^2qQ/h is the static quadrupolar coupling constant, and for the completely static C_α–^{2}H bond, the value of $(3/2)(e^2qQ/h)$ is approximately 250 kHz (Barnes & Bloom, 1973; Oldfield et al., 1982). The angle β' is the angle between the axis of motional averaging and the direction of the magnetic field. The symbols $\langle\ \rangle$ denote a time average over motions occurring during the time scale of the NMR measurement. Therefore, the quadrupolar splitting $\Delta\nu_Q$ characterizes a conformational and dynamical state of the C–^{2}H bond in which the C–^{2}H bond undergoes certain motions and adopts certain conformations during the time scale of the NMR measurement. An important point to consider, though, is that different conformational and dynamical states of the C–^{2}H bond may be characterized by the same quadrupolar splitting.

At temperatures above the phase transition temperature, the quadrupolar splitting of the main deuterium resonance lines varies with sample orientation in such a way that the quadrupolar splitting measured at β = 0° is twice the magnitude of the quadrupolar splitting measured at β = 90° (Table II). This result and the reduced magnitude of $\Delta\nu_Q$ indicate that

the Ala[3] residue of the gramicidin backbone rotates rapidly about an axis parallel to the normal to the glass coverslips. Specifically, the values of $|\Delta\nu_Q|$ for $\beta = 0°$ and $\beta = 90°$ measured from the spectra of Figures 3a,b,f,g and tabulated in Table II obey eq 2 if the axis of motional averaging is parallel to the normal to the glass coverslips, in other words, if $\beta' = \beta$.

For those deuterium nuclei that can be observed, only the magnitude of the quadrupolar splitting can be measured from the frequency difference between the two main resonance lines. However, although the sign of $\Delta\nu_Q$ cannot be obtained directly from the spectrum, the sign of $\Delta\nu_Q$ can sometimes be deduced from other considerations (Seelig, 1977). For the values of $|\Delta\nu_Q|$ obtained above the phase transition temperature in Tables II and III, eq 2 shows that the sign of $\Delta\nu_Q$ can be determined because the absolute value of $\langle(3\cos^2\theta - 1)/2\rangle$ must be greater than $^1/_2$ to produce the measured absolute values of $\Delta\nu_Q$ given that $(^3/_2)(e^2qQ/h) = 250$ kHz, and this is only possible if $\langle(3\cos^2\theta - 1)/2\rangle$ is positive.

At temperatures near and above the phase transition temperture, the magnitude of the ^{2}H quadrupolar splitting $\Delta\nu_Q$ of the observable Ala[3] C_α–^{2}H bonds is reduced relative to that expected for a completely static C_α–^{2}H bond and increases slightly with decreasing temperature (Table III). As pointed out before, the reduced magnitude of the quadrupolar splitting $\Delta\nu_Q$ represents a conformational and dynamical state of the C_α–^{2}H bond in which many conformations or motions may be sampled during the time scale of the NMR measurement. If, however, the only motion that occurs is fast rotation about a given axis, then in eq 2 the term $\langle(3\cos^2\theta - 1)/2\rangle$ becomes equal to $(3\cos^2\theta - 1)/2$; in this case, a meaningful conformational angle θ between the motional axis and the C_α–^{2}H bond can be calculated directly from the reduced magnitude of $\Delta\nu_Q$ and eq 2. Given a value of 250 kHz for $(^3/_2)(e^2qQ/h)$ and the measured values of $|\Delta\nu_Q|$ near and above the phase transition temperature (Tables II and III), eq 2 yields a value of $\theta = 20°$ at $T = 44$ °C and a value of $\theta = 19°$ at $T = 24$ °C for the angle between the axis of motional averaging and the Ala[3] C_α–^{2}H bond. The values obtained for θ therefore indicate that the C_α–^{2}H bond of the Ala[3] residue undergoes a conformational change relative to the axis of motional averaging as the temperature is decreased if the only motion present is fast axial rotation. Such a conformational change, even if it does occur, is relatively small. However, another explanation for the observed increase in the magnitude of $\Delta\nu_Q$ with decreasing temperature is that the dynamics of the C_α–^{2}H bond change slightly as the temperature decreases. Motions that may influence the magnitude of $\Delta\nu_Q$ as the temperature changes include small-amplitude, high-frequency motions of the C_α–^{2}H bond and fluctuations in the orientation of the motional axis (Davis, 1988). Possibly, the temperature may ultimately exert its effect on $\Delta\nu_Q$ through temperature-dependent changes in membrane thickness or membrane fluidity.

Distribution of Orientations. An analysis of the line width of the observed deuterium resonance lines yields information about the distribution of Ala[3] C_α–^{2}H bond orientations about some mean orientation. At temperatures above the phase transition temperature, the resonance line width of those deuterium nuclei that can be observed is relatively narrow and does not show a significant dependence on macroscopic sample orientation (Table II). In terms of symmetry, an individual resonance line exhibits a slight asymmetry at temperatures above the phase transition temperature which is apparent as an increased intensity at the base of the resonance line on the side closest to the center of the spectrum. Although the spectra obtained with $\tau = 200$ μs exhibit this asymmetry to a small degree, this asymmetry is most apparent in the spectra obtained with $\tau = 60$ μs. These results can be interpreted in terms of inhomogeneous line broadening that arises from C_α–^{2}H bonds not all possessing the same motional axis orientation relative to the coverslip normal. Most likely, a distribution of motional axis orientations exists in which most motional axes are aligned parallel to the coverslip normal. Equation 2 shows how such a distribution of C_α–^{2}H bond motional axis orientations translates into a frequency spectrum. In particular, such a distribution of C_α–^{2}H bond motional axis orientations can only give rise to quadrupolar splittings smaller in magnitude than $\Delta\nu_Q(\beta' = 0°)$ for the $\beta = 0°$ orientation and quadrupolar splittings smaller in magnitude than $\Delta\nu_Q(\beta' = 90°)$ for the $\beta = 90°$ orientation. This explanation agrees with the data obtained above the phase transition temperature in the sense that the base of the resonance line is increased slightly in intensity toward the center of the spectrum. Furthermore, eq 2 can be used to estimate the width of the distribution of β' angles from the line width of the resonance. If this estimate is based on the half-width at half-intensity of the resonance line, then the distribution of β' angles for the Ala[3] C_α–^{2}H bond in the DMPC–gramicidin sample at temperatures above the phase transition temperature has a width of approximately 2° for the $\beta = 0°$ sample orientation.

Inhomogeneous line broadening may also arise from a distribution of C_α–^{2}H bond conformations relative to the motional axis. Equation 2 shows that such a distribution gives rise to quadrupolar splittings measurably smaller and larger in magnitude than the main quadrupolar splitting for any appreciable spread in θ. The deuterium spectra acquired above the phase transition temperature, however, do not provide significant evidence for the existence of such a distribution.

Homogeneous line-broadening mechanisms may also be important in determining the line width of the observable deuterium nuclei at temperatures above the phase transition temperature; if this is the case, then the previous estimate of the width of the distribution of motional axis orientations from the observed line width is likely to be too large. A potential source of homogeneous line broadening is the intermolecular and intramolecular magnetic dipolar interactions between an observed deuterium nucleus and the surrounding protons. However, line broadening due to dipolar interactions should not be reflected in the spectra obtained above the phase transition temperature because lateral diffusion removes the effect of intermolecular dipolar interactions and proton decoupling removes the effect of intramolecular dipolar interactions in the liquid-crystalline phase. Other sources of homogeneous line broadening such as fluctuations of the electric quadrupolar interaction may be present though.

Number of Conformational and Dynamical States. The number of resonance lines present in the deuterium spectra obtained above the phase transition temperature allow conclusions to be drawn about the number of Ala[3] C_α–^{2}H bond conformational and dynamical states observable at these temperatures. The spectra of Figure 3 show that most of the observable deuterium signal is concentrated in two main resonance lines at temperatures near and above the phase transition temperature. The fact that only one quadrupolar splitting is apparent in the NMR spectrum for a given sample orientation indicates that only one major conformational and dynamical state is likely to exist for those Ala[3] C_α–^{2}H bonds that can be observed. This does not preclude the existence of other conformational and dynamical states of the Ala[3] C_α–^{2}H bond, but the population or the NMR relaxation of

the C_α–^{2}H bonds in each of these other states must prevent the corresponding ^{2}H NMR signal from becoming apparent above the noise of the NMR spectrum; otherwise, several different quadrupolar splittings are expected to be present in a single spectrum. Furthermore, if the only motion present is simple axial rotation, then the quadrupolar splitting $\Delta\nu_Q$ represents a conformational and dynamical state in which the Ala[3] C_α–^{2}H bond maintains a single, unchanging, bond conformation relative to the motional axis. In this case, the observation of one major quadrupolar splitting in the observed spectra implies that only one major bond conformation exists for the Ala[3] C_α–^{2}H bond.

A component corresponding to a random orientation of motional axes of the C_α–^{2}H bond gives rise to a line shape similar to the powder line shapes shown in Figure 2, but the separation between the main peaks for the membrane sample is given by $\Delta\nu_Q(\beta' = 90°)$ which in this case is the value of $\Delta\nu_Q$ measured for the $\beta = 90°$ sample orientation. Consequently, the line shape signifying the presence of a randomly oriented component is expected to be most apparent in the spectrum obtained at $\beta = 0°$. Examination of Figure 3a shows that a line shape indicating the presence of such a component may possibly exist, but the signal to noise ratio of the spectrum does not permit any definite conclusions to be drawn.

Each of the spectra in Figure 3 does exhibit, though, a peak located at the center of the spectrum. The intensity of this center peak shows a small dependence on temperature. As the temperature approaches the phase transition temperature from higher or lower temperatures, the intensity of the center peak increases. Moreover, the line width of the center peak appears to show a small dependence on sample orientation at $T = 44$ and 4 °C. This suggests that the center peak has a physical origin and is not just a systematic spectral artifact. Several possible physical explanations of the center peak exist. One possible explanation of the center peak is that it reflects the formation of a motionally isotropic phase, even though ^{31}P NMR spectra of the sample at the same temperature and orientation do not indicate the presence of such a phase for the lipid matrix. A second possible explanation of the center peak is that it arises from Ala[3] C_α–^{2}H bonds oriented at the magic angle with respect to the axis of motional averaging. Equation 2 shows that such an orientation ($\theta = 54.7°$) collapses the quadrupolar splitting to zero for all macroscopic orientations. However, the temperature dependence of the intensity of the center peak is qualitatively different from that of the main deuterium resonance lines representing the gramicidin molecules. This suggests that the center peak does not arise from a different conformational state of gramicidin. A third and more likely explanation of the center peak is that it arises from deuterium in water, even though deuterium-depleted water is used in most of the sample preparation steps.

Gel Phase. The absence of a signal for the $\beta = 0°$ sample orientation at temperatures below the phase transition temperature indicates that gramicidin is still ordered at the molecular level in the gel phase. Also, the observation of a quadrupolar splitting that approaches 123 kHz in magnitude at the extreme edges of the resonance lines for the $\beta = 90°$ sample orientation is consistent with the C_α–^{2}H bond of the gramicidin molecule being largely immobile in the gel phase on the ^{2}H NMR time scale. Deuterium NMR spectra consistent with immobilization of the gramicidin molecule in the gel phase have been observed before (Datema et al., 1986; Macdonald & Seelig, 1988). However, a quantitative analysis of C_α–^{2}H bond orientations in the gel phase for the sample studied here requires a better signal to noise ratio for the spectrum corresponding to $\beta = 90°$ or the observation of a signal for the spectrum corresponding to $\beta = 0°$.

Discussion

Peptide Synthesis

The solid-phase method of peptide synthesis allows the amino acids comprising the Val[1]···(2-^{2}H)Ala[3]···gramicidin A peptide to be linked together quickly and easily. Purification of the crude product by countercurrent chromatography and preparative TLC allows a pure, final product to be obtained. Characterization of the final Val[1]···(2-^{2}H)Ala[3]···gramicidin A product to verify its purity is important because the presence of impurities could hypothetically affect many aspects of the DMPC–gramicidin system, thereby complicating or rendering meaningless the observed ^{2}H NMR spectrum. While the particular procedure used here for construction and purification of the peptide can be improved upon, the quantity produced is sufficient for this particular solid-state NMR study.

Sample Preparation

The preparation of the sample is an important step in the experiment because experimental conditions must be chosen so as to give a high probability of obtaining the channel conformation. The choice of DMPC as the lipid matrix, the mixing of DMPC and gramicidin in a 10:1 molar ratio in methanol, and the subsequent heating of the sample at elevated temperatures for an extended period of time should allow gramicidin to adopt a conformation interpretable as that of the functional channel because circular dichroism has shown that these conditions are compatible with the formation of such a conformation (Wallace et al., 1981; Nicholson et al., 1987). Although evidence exists that the use of methanol in the cosolubilizing solvent may predispose gramicidin to form a nonfunctional dimeric structure, the subsequent heating step should convert the nonfunctional dimeric structures, if any have formed, to the functional channel structure (Killian et al., 1988; Killian & Urry, 1988). Also, the addition of water to the solution from which the DMPC–gramicidin mixture is deposited helps ensure that the DMPC–gramicidin mixture deposits in the proper way.

However, the definitive experiment to demonstrate that gramicidin is incorporated as a functional channel in the unmodified, solid-state NMR sample has not yet been performed. Nevertheless, the observation of a quadrupolar splitting representing a major conformational and dynamical state of gramicidin in DMPC is important because this helps define the conformations that gramicidin can adopt in a lipid environment.

Molecular Conformation

The most important information to be gained from a solid-state NMR study of this DMPC–gramicidin system is information about the molecular conformation of gramicidin in relation to the bilayer as a whole. Information about the lipid matrix is provided by the ^{31}P NMR spectra which show that the DMPC headgroup rotates about an axis parallel to the coverslip normal. This type of lipid headgroup motion in oriented phospholipid mixtures has been observed on numerous occasions (McLaughlin et al., 1975; Seelig & Gally, 1976; Hemminga & Cullis, 1982) and, more recently, has also been observed for an oriented DMPC–gramicidin sample (Nicholson et al., 1987). This motion is consistent with the presence of a bilayer phase in which the phospholipid molecules rotate about their long axes. In this case, the long axes of the lipid molecules are arranged parallel to the coverslip normal, thereby implying that the surface of the bilayer is parallel to

the surface of the glass coverslips. In a similar way, the ^2H NMR spectra show that the Ala^3 residue of gramicidin also rotates about an axis parallel to the coverslip normal in the liquid-crystalline phase. This type of gramicidin motion in an oriented DMPC–gramicidin mixture has been observed before (Cornell et al., 1988). If gramicidin adopts a helical structure in the membrane and axial rotation occurs about the helical axis, then the helical axes of the gramicidin molecules are parallel to the coverslip normal and to the long axes of the lipid molecules. This provides an indication of how the gramicidin molecules are most probably intercalated into the lipid bilayer in the liquid-crystalline phase.

Furthermore, the assumption that gramicidin forms a helical structure and rotates about the helical axis in the bilayer allows the angle θ between the C_α–^2H bond and the motional axis to be interpreted as the angle between the C_α–^2H bond and the helical axis. If fast axial rotation is assumed to be the only motion that occurs, then the observed quadrupolar splittings yield values of 19–20° for the angle between the Ala^3 C_α–^2H bond and the helical axis in the liquid-crystalline phase.

The experimentally derived angle between the Ala^3 C_α–^2H bond and the helical axis can now be used to evaluate various theoretical models of the gramicidin channel. The theoretical models to be considered can be divided into two classes: double-stranded, helical dimers and single-stranded, helical dimers. These models are evaluated by calculation of Ala^3 C_α–^2H bond angles relative to the helical axis and comparison of these theoretical predictions with the experimental data. One point to consider, though, is that slight variations in the structure of a single model may result in a number of different values for the angle between the Ala^3 C_α–^2H bond and the helical axis; therefore, a range of theoretical bond angles for the Ala^3 C_α–^2H bond may need to be considered for a single model. A second point to consider is that each of the theoretical models to be considered possesses a twofold symmetry axis either perpendicular or parallel to the helical axis so that the bond angle relative to the helical axis for the Ala^3 C_α–^2H bond on one monomer is the same as the bond angle for the corresponding, chemically identical Ala^3 C_α–^2H bond on the other monomer; consequently, bond angle calculations for the Ala^3 C_α–^2H bond need only be performed for one monomer.

The double-stranded, helical dimer models to be considered include the left-handed, antiparallel, $\beta\beta^{5,6}$ helical dimer (species 3); the right-handed, parallel, $\beta\beta^{5,6}$ helical dimer (species 4); the left-handed, parallel, $\beta\beta^{5,6}$ helical dimer that is the mirror image of species 4 (species 1); and the right-handed, antiparallel, $\beta\beta^{7,2}$ helical dimer (Veatch et al., 1974; Prasad & Chandrasekaran, 1977; Colonna-Cesari et al., 1977; Arseniev et al., 1984, 1985a; Bystrov & Arseniev, 1988). Preliminary calculations performed on these models indicate that the angle between the Ala^3 C_α–^2H bond and the helical axis is ≈30–40°; the exact value obtained for the bond angle depends on the particular model chosen for the calculation. In any case, these models predict bond angles that are larger than the angle derived from the experimental data; in other words, the theoretical bond angles correspond to quadrupolar splittings that are smaller in magnitude than the observed quadrupolar splitting. Thus, under the assumption that fast axial rotation is the only motion present, the experimentally derived Ala^3 C_α–^2H bond angle indicates that the double-stranded, helical dimer models are very unlikely to represent the structure of gramicidin in the DMPC–gramicidin sample studied in this paper.

In terms of the single-stranded, $\beta^{6,3}$ helical dimer models (Urry, 1971; Urry et al., 1971; Arseniev, 1985b; Venkatachalam & Urry, 1983), preliminary calculations show that the Ala^3 C_α–^2H bond angle relative to the helical axis is ≈14–18° in the left-handed model, while the Ala^3 C_α–^2H bond angle relative to the helical axis is ≈10–14° in the right-handed model. Again, the exact value calculated for the bond angle depends on the details of the model chosen for the calculation, but the Ala^3 C_α–^2H bond angle derived from the left-handed model tends to be a few degrees larger than the Ala^3 C_α–^2H bond angle derived from the right-handed model. Thus, under the assumption that fast axial rotation is the only motion present, the experimentally derived Ala^3 C_α–^2H bond angle of 19–20° is within range of the predictions of the single-stranded, $\beta^{6,3}$ helical dimer models but is in slightly closer agreement with the bond angles derived from the left-handed, single-stranded, $\beta^{6,3}$ helical dimer model than with the bond angles derived from the right-handed model. However, the small, theoretical difference between the left-handed and right-handed models in terms of the Ala^3 C_α–^2H bond angle does not really permit the left-handed model to be definitively distinguished from the right-handed model on the basis of the experimental data obtained so far.

If the assumption made in the preceding discussion that the only motion present is fast axial rotation is not valid and motions other than fast axial rotation are present which also partially average the quadrupolar splitting, then these motions must also be taken into account when the measured quadrupolar splitting is interpreted. In the absence of specific motional models, though, the most information that can be extracted from the measured quadrupolar splitting is the maximum possible angular deviation between the Ala^3 C_α–^2H bond and the helical axis. This is because motions that partially average the quadrupolar splitting other than fast axial rotation cause the measured quadrupolar splitting to be smaller in magnitude than the quadrupolar splitting that reflects only bond angle information. In this case, eq 2 and the large magnitude of the measured quadrupolar splitting show that the actual bond angle must be smaller than the one calculated from the measured quadrupolar splitting, and so 19–20° is the maximum angle that the Ala^3 C_α–^2H bond can make with the helical axis in the liquid-crystalline phase. For the various theoretical models of gramicidin structure, the implications of the Ala^3 C_α–^2H bond angle possessing an upper limit of 19–20° are essentially the same as the implications of the Ala^3 C_α–^2H bond angle possessing a value of 19–20°. For the double-stranded, helical dimer models, the 19–20° upper limit of the Ala^3 C_α–^2H bond angle indicates that these models are very unlikely to represent the structure of gramicidin in the sample studied in this paper. For the single-stranded, $\beta^{6,3}$ helical dimer models, the 19–20° upper limit of the Ala^3 C_α–^2H bond angle is consistent with both the left-handed and right-handed models with the distinction between the two models now being even harder to make.

Distribution of Orientations

Another important aspect to consider about the system studied in this paper is the distribution of gramicidin Ala^3 C_α–^2H bond orientations about some mean orientation relative to the distribution of DMPC headgroup orientations about some mean orientation. In particular, two types of orientational distributions need to be considered: a distribution of conformations relative to the motional axis and a distribution of motional axis orientations relative to the coverslip normal. Since these two types of distributions give rise to different line shapes for the sample orientations studied in this paper, their relative contributions can be assessed by examining the line shape. Also, the distribution of motional axis orientations is

more likely to be directly affected by the sample preparation conditions and so is more likely to vary from experiment to experiment.

For the ^{31}P NMR spectra, the line width, intensity, and symmetry of the main resonance line are all consistent with the presence of a distribution of motional axis orientations; this distribution possesses an estimated width of ~7° in the liquid-crystalline phase. Likewise, the symmetry of the main deuterium resonance lines indicates that a distribution of motional axis orientations is more important in contributing to the observed line width. In this case, the width of the distribution of Ala[3] motional axis orientations is estimated to be 2° in the liquid-crystalline phase. That the DMPC headgroup is estimated to have a wider range of motional axis orientations than the gramicidin Ala[3] residue at temperatures above the phase transition temperature can be explained in several ways. One explanation for this result is that the distributional width of motional axis orientations is actually wider for the headgroup of the phospholipid molecules than for the gramicidin molecules. This implies that the gramicidin helices are more ordered in the bilayer than are the phospholipid headgroups. A second explanation for the difference in estimated distributional widths is that the estimate of the distributional width of motional axis orientations for the DMPC headgroup is not as accurate as that for the Ala[3] C_α–^{2}H bond, possibly because of the need to estimate the amount of homogeneous line broadening present in the phosphorus spectra.

Number of Conformational and Dynamical States

A third important aspect to consider about the DMPC–gramicidin system studied in this paper is the number of different types of conformational and dynamical states that the gramicidin molecules can assume. Given that the center peak in the deuterium spectra is most likely deuterium in water, the observation of one major quadrupolar splitting for the sample in the liquid-crystalline phase indicates that only one major conformational and dynamical state is likely to exist above the phase transition temperature for those Ala[3] C_α–^{2}H bonds that can be observed. If the observed Ala[3] C_α–^{2}H bonds represent all the Ala[3] C_α–^{2}H bonds in the sample, then the implications of observing one major quadrupolar splitting are several.

If monomers and dimers are both present in the sample in significant amounts, then their lifetimes (Hladky & Haydon, 1972) should permit them to be observable as distinct species by NMR; in this case, the observation of one major quadrupolar splitting implies that no significant differences are likely to exist between monomers and dimers in the conformational and dynamical state of the Ala[3] C_α–^{2}H bond. If, on the other hand, only one species is present in the sample in significant amounts, then of course no conclusions can be reached about possible conformational and dynamical differences between monomers and dimers.

If minor conducting forms are present in the sample in significant amounts, then their lifetimes (Busath & Szabo, 1981) should permit them to be observable as distinct species by NMR; in this case, the observation of one major quadrupolar splitting implies that no significant differences are likely to exist between conducting forms in the conformational and dynamical state of the Ala[3] C_α–^{2}H bond. If, on the other hand, minor conducting forms are not prevalent enough to be observable by NMR, then of course no conclusions can be reached about possible conformational and dynamical differences between conducting forms.

Moreover, if simple axial rotation is the only motion that the gramicidin molecule undergoes, then the previous statements reduce to the statement that no significant differences exist in the conformation of the Ala[3] C_α–^{2}H bond between monomers and dimers or between various conducting forms if these species are present in the sample in significant amounts.

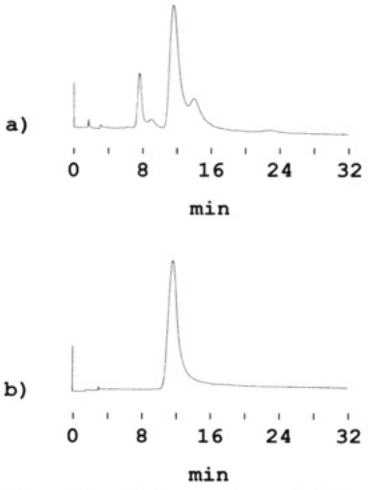

FIGURE 6: HPLC profile of (a) natural gramicidin and (b) Val[1]···(2-^{2}H)Ala[3]···gramicidin A eluted isocratically from a Vydac C_4 column at 1 mL/min with 63.5% methanol in water and detected at 214 nm with a sensitivity of 0.1 aufs. The sample is dissolved in methanol at a concentration of 1 μg/μL and injected into the column in a volume of 2 μL.

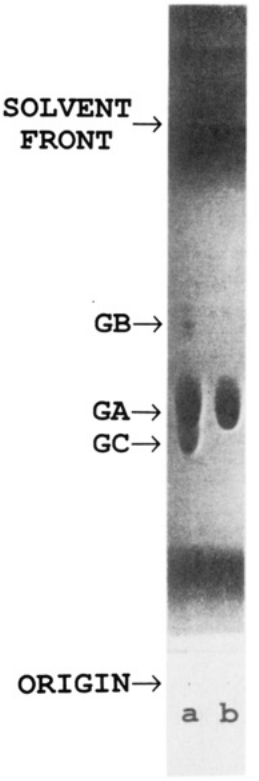

FIGURE 7: TLC deposition of (a) natural gramicidin and (b) Val[1]···(2-^{2}H)Ala[3]···gramicidin A onto a Whatman LK5, silica gel 80-Å, 250-μm TLC plate. The sample is dissolved in methanol at a concentration of 6 μg/μL, deposited onto the plate in a volume of 2 μL, developed with chloroform/methanol/acetic acid (85:15:3), and visualized by exposure to iodine vapors.

Appendix: Peptide Characterization

Characterization of the final Val[1]···(2-^{2}H)Ala[3]···gramicidin A product by HPLC, TLC, ^{13}C NMR, ^{1}H NMR, mass spectrometry, and amino acid analysis results in the data shown in Figures 6–9 and Table IV. In general, characterization

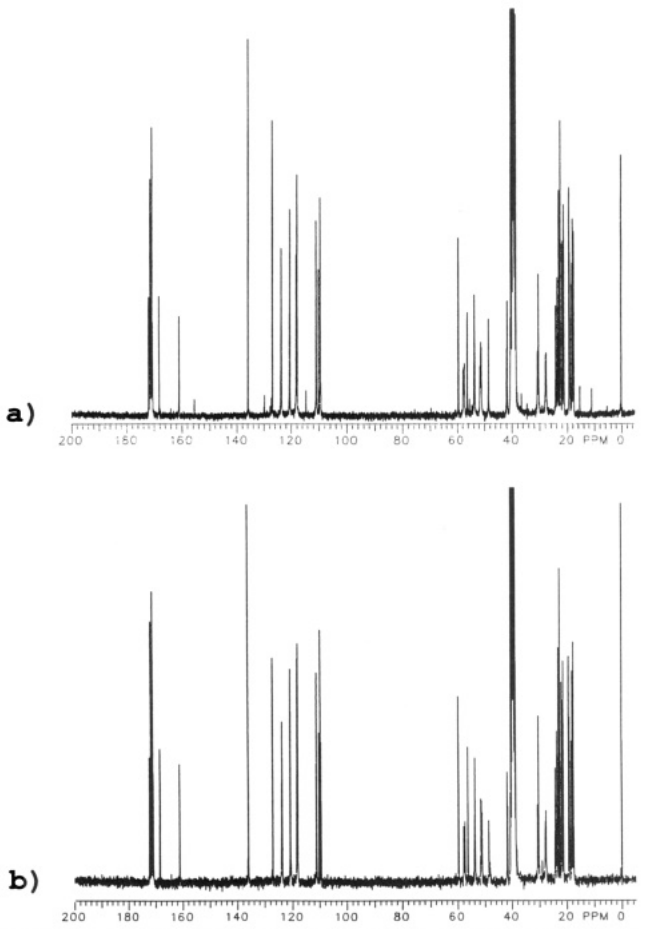

FIGURE 8: 75-MHz ^{13}C NMR spectra of (a) natural gramicidin at a concentration of 249 mg/mL (12000 scans) and (b) Val^1···(2-^{2}H)Ala^3···gramicidin A at a concentration of 100 mg/mL (13850 scans). Samples are dissolved in ($^2H_6$)dimethyl sulfoxide with 1% tetramethylsilane. Spectra are recorded with a Varian XL300 spectrometer at room temperature with a deuterium lock and proton decoupling and are referenced to tetramethylsilane.

Table IV: Amino Acid Analysis[a] of Natural Gramicidin and Val^1···(2-^{2}H)Ala^3···Gramicidin A

	natural gramicidin		Val^1···(2-^{2}H)-Ala^3···GA	
amino acid	expt	theory	expt	theory
glycine	1.05	1.00	1.14	1.00
alanine	2.06	2.00	1.89	2.00
valine	3.67	3.86[b]	3.79	4.00
isoleucine	0.08	0.14[b]	0.00	0.00
leucine	4.00	4.00	4.00	4.00
tyrosine	0.23	0.19[c]	0.00	0.00
phenylalanine	0.00	0.09[c]	0.00	0.00

[a] Hydrolysis is performed for 4 h at 145 °C in hydrochloric acid/propionic acid with 0.1% phenol; hydrolysate is redissolved in a 0.2 M sodium citrate buffer of pH 2.2, injected onto a Beckman Model 6300 amino acid analyzer that resolves amino acids by ion exchange, eluted according to the manufacturer's protocols, and detected by a postcolumn ninhydrin method at 440 and 570 nm. [b] Based on amounts of Val^1···GA, Ile^1···GA, Val^1···GC, and Ile^1···GC obtained from natural gramicidin by countercurrent chromatography performed on a coil planet centrifuge. [c] Based on a ratio of 72:9:19 for GA:GB:GC (Glickson et al., 1972).

of the Val^1···(2-^{2}H)Ala^3···gramicidin A product by the aforementioned techniques results in confirmation of the identity of the product and of the high purity of the product.

Characterization of the product by HPLC results in the chromatograms shown in Figure 6. Figure 6a is the chromatogram of natural gramicidin (ICN) and shows that the components of natural gramicidin can be identified under these

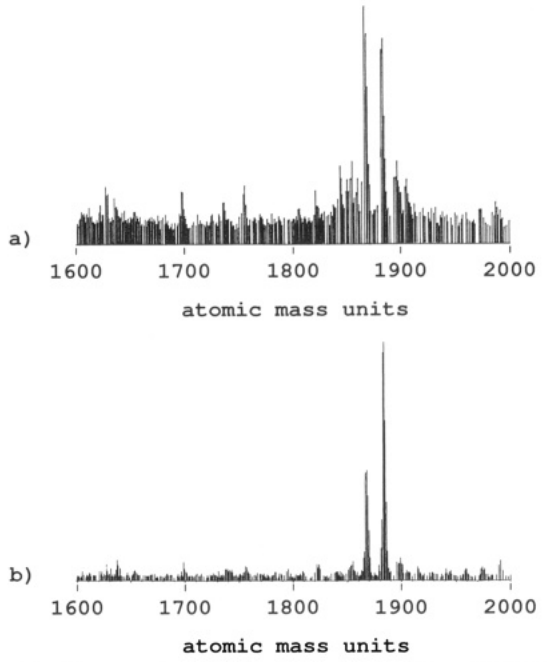

FIGURE 9: Mass spectra of (a) natural gramicidin and (b) Val^1···(2-^{2}H)Ala^3···gramicidin A. Mass spectra of gramicidin are acquired with a VG ZAB-SE mass spectrometer by fast atom bombardment.

HPLC conditions (Urry et al., 1983b). Figure 6b is the chromatogram of synthetic Val^1···(2-^{2}H)Ala^3···gramicidin A and indicates that the synthetic gramicidin possesses the same retention time as the corresponding natural Val^1···gramicidin A component and that the synthetic product is of high purity.

Analytical TLC performed on the final product results in the thin-layer chromatogram shown in Figure 7. On the left side of Figure 7, the major components of natural gramicidin deposit onto the TLC plate in the same order as they elute from the HPLC column. On the right side of Figure 7, the Val^1···(2-^{2}H)Ala^3···gramicidin A product is shown to deposit onto the TLC plate with the same R_f value as its natural counterpart. Also, the existence of only one TLC spot for the synthetic gramicidin indicates the high purity of the product.

Figure 8 shows the ^{13}C NMR spectra of natural gramicidin and Val^1···(2-^{2}H)Ala^3···gramicidin A. Figure 8a shows the ^{13}C NMR spectrum of natural gramicidin; the assignments of these resonances to specific carbon atoms have been made previously by others (Fossel et al., 1974; Prasad et al., 1982). Figure 8b shows the ^{13}C NMR spectrum of Val^1···(2-^{2}H)Ala^3···gramicidin A. This spectrum shows that Val^1···(2-^{2}H)Ala^3···gramicidin A possesses the same resonances as the Val^1···gramicidin A component of the natural mixture, thereby providing further evidence as to the identity of the synthetic product. Also, no major impurities are detected in the spectrum of Figure 8b.

Mass spectra of natural gramicidin and the synthetic product are shown in Figure 9. The mass spectrum of natural gramicidin (Figure 9a) contains peaks centered about a peak of 1883 atomic mass units and peaks centered about a peak of 1867 atomic mass units. The peak at 1883 is consistent with the molecular weight of the Val^1···gramicidin A component of the natural mixture (1882), and a peak appearing 16 atomic mass units lower than the peak representing the molecular weight appears to be a characteristic feature of mass spectra of gramicidin obtained under these conditions. In any case, the mass spectrum of Val^1···(2-^{2}H)Ala^3···gramicidin A (Figure 9b) shows the same basic pattern as that of Val^1···gramicidin A except that one set of peaks is now centered about 1884, which is consistent with the 1883 molecular weight of Val^1···(2-^{2}H)Ala^3···gramicidin A.

The amino acid analysis of the final product is displayed in Table IV. Since the conditions under which the amino acid analysis is performed destroy tryptophan side chains, the tryptophan content of gramicidin cannot be assessed in this case. For the other amino acids, however, Table IV shows that they are present in approximately the correct ratio for Val[1]···(2-^{2}H)Ala[3]···gramicidin A.

Acknowledgments

Thanks to Tony Biondo, Todd Hardt, Mark Mueller, and Denny Kyle for physical construction of the NMR probe. Thanks to Eric Kolodziej and Paul Toren for obtaining the mass spectra. Thanks to Jim Zobel for performing the amino acid analysis. Thanks to Dan Urry for providing the atomic coordinates of the left-handed, single-stranded, $\beta^{6.3}$ helical dimer. Thanks to Wan Lau for calculating the atomic coordinates of the various theoretical models of gramicidin structure.

References

Arseniev, A. S., Bystrov, V. F., Ivanov, V. T., & Ovchinnikov, Y. A. (1984) *FEBS Lett. 165*, 51–56.

Arseniev, A. S., Barsukov, I. L., & Bystrov, V. F. (1985a) *FEBS Lett. 180*, 33–39.

Arseniev, A. S., Barsukov, I. L., Bystrov, V. F., Lomize, A. L., & Ovchinnikov, Y. A. (1985b) *FEBS Lett. 186*, 168–174.

Barnes, R. G., & Bloom, J. W. (1973) *Mol. Phys. 25*, 493–494.

Beshah, K., Olejniczak, E. T., & Griffin, R. G. (1987) *J. Chem. Phys. 86*, 4730–4736.

Busath, D., & Szabo, G. (1981) *Nature 294*, 371–373.

Bystrov, V. F., & Arseniev, A. S. (1988) *Tetrahedron 44*, 925–940.

Chapman, D., Urbina, J., & Keough, K. M. (1974) *J. Biol. Chem. 249*, 2512–2521.

Chapman, D., Cornell, B. A., Eliasz, A. W., & Perry, A. (1977) *J. Mol. Biol. 113*, 517–538.

Colonna-Cesari, F., Premilat, S., Heitz, F., Spach, G., & Lotz, B. (1977) *Macromolecules 10*, 1284–1288.

Cornell, B. A., Separovic, F., Baldassi, A. J., & Smith, R. (1988) *Biophys. J. 53*, 67–76.

Datema, K. P., Pauls, K. P., & Bloom, M. (1986) *Biochemistry 25*, 3796–3803.

Davis, J. H. (1988) *Biochemistry 27*, 428–436.

Fields, G. B., Fields, C. G., Petefish, J., Van Wart, H. E., & Cross, T. A. (1988) *Proc. Natl. Acad. Sci. U.S.A. 85*, 1384–1388.

Fontana, A., & Gross, E. (1972) *Pept., Proc. Eur. Pept. Symp., 12th, 1972*, 229–234.

Fossel, E. T., Veatch, W. R., Ovchinnikov, Y. A., & Blout, E. R. (1974) *Biochemistry 13*, 5264–5275.

Glickson, J. D., Mayers, D. F., Settine, J. M., & Urry, D. W. (1972) *Biochemistry 11*, 477–486.

Gregory, J. D., & Craig, L. C. (1948) *J. Biol. Chem. 172*, 839–840.

Griffin, R. G. (1981) *Methods Enzymol. 72*, 108–174.

Hemminga, M. A., & Cullis, P. R. (1982) *J. Magn. Reson. 47*, 307–323.

Hing, A. W. (1990) Ph.D. Thesis, Washington University, St. Louis, MO.

Hladky, S. B., & Haydon, D. A. (1970) *Nature 225*, 451–453.

Hladky, S. B., & Haydon, D. A. (1972) *Biochim. Biophys. Acta 274*, 294–312.

Hotchkiss, R. D., & Dubos, R. J. (1941) *J. Biol. Chem. 141*, 155–162.

Hoult, D. I., & Richards, R. E. (1975) *Proc. R. Soc. London A 344*, 311–340.

Ito, Y. (1986) *CRC Crit. Rev. Anal. Chem. 17*, 65–143.

Ito, Y., Sandlin, J., & Bowers, W. G. (1982) *J. Chromatogr. 244*, 247–258.

Killian, J. A., & Urry, D. W. (1988) *Biochemistry 27*, 7295–7301.

Killian, J. A., Prasad, K. U., Hains, D., & Urry, D. W. (1988) *Biochemistry 27*, 4848–4855.

Levitt, M. H., Suter, D., & Ernst, R. R. (1984) *J. Chem. Phys. 80*, 3064–3068.

Macdonald, P. M., & Seelig, J. (1988) *Biochemistry 27*, 2357–2364.

McLaughlin, A. C., Cullis, P. R., Hemminga, M. A., Hoult, D. I., Radda, G. K., Ritchie, G. A., Seeley, P. J., & Richards, R. E. (1975) *FEBS Lett. 57*, 213–218.

Merrifield, R. B. (1963) *J. Am. Chem. Soc. 85*, 2149–2154.

Nicholson, L. K., Moll, F., Mixon, T. E., LoGrasso, P. V., Lay, J. C., & Cross, T. A. (1987) *Biochemistry 26*, 6621–6626.

Niederberger, W., & Seelig, J. (1976) *J. Am. Chem. Soc. 98*, 3704–3706.

Noda, K., & Gross, E. (1972) in *Chemistry and Biology of Peptides* (Meienhofer, J., Ed.) pp 241–250, Ann Arbor Science Publishers, Ann Arbor, MI.

Oldfield, E., Kinsey, R. A., & Kintanar, A. (1982) *Methods Enzymol. 88*, 310–325.

Pauls, K. P., MacKay, A. L., Soderman, O., Bloom, M., Tanjea, A. K., & Hodges, R. S. (1985) *Eur. Biophys. J. 12*, 1–11.

Pines, A., Chang, J. J., & Griffin, R. G. (1974) *J. Chem. Phys. 61*, 1021–1030.

Prasad, B. V. V., & Chandrasekaran, R. (1977) *Int. J. Pept. Protein Res. 10*, 129–138.

Prasad, K. U., Trapane, T. L., Busath, D., Szabo, G., & Urry, D. W. (1982) *Int. J. Pept. Protein Res. 19*, 162–171.

Rajan, S., Kang, S.-Y., Gutowsky, H. S., & Oldfield, E. (1981) *J. Biol. Chem. 256*, 1160–1166.

Sarges, R., & Witkop, B. (1965a) *J. Am. Chem. Soc. 87*, 2011–2020.

Sarges, R., & Witkop, B. (1965b) *J. Am. Chem. Soc. 87*, 2027–2030.

Sarges, R., & Witkop, B. (1965c) *Biochemistry 4*, 2491–2494.

Seelig, J. (1977) *Q. Rev. Biophys. 10*, 353–418.

Seelig, J. (1978) *Biochim. Biophys. Acta 515*, 105–140.

Seelig, J., & Gally, H.-U. (1976) *Biochemistry 15*, 5199–5204.

Seelig, J., Borle, F., & Cross, T. A. (1985) *Biochim. Biophys. Acta 814*, 195–198.

Spiess, H. W., & Sillescu, H. (1981) *J. Magn. Reson. 42*, 381–389.

Stejskal, E. O., & Schaefer, J. (1974) *J. Magn. Reson. 14*, 160–169.

Urry, D. W. (1971) *Proc. Natl. Acad. Sci. U.S.A. 68*, 672–676.

Urry, D. W., Goodall, M. C., Glickson, J. D., & Mayers, D. F. (1971) *Proc. Natl. Acad. Sci. U.S.A. 68*, 1907–1911.

Urry, D. W., Prasad, K. U., & Trapane, T. L. (1982a) *Proc. Natl. Acad. Sci. U.S.A. 79*, 390–394.

Urry, D. W., Walker, J. T., & Trapane, T. L. (1982b) *J. Membr. Biol. 69*, 225–231.

Urry, D. W., Trapane, T. L., & Prasad, K. U. (1983a) *Science 221*, 1064–1067.

Urry, D. W., Trapane, T. L., Romanowski, S., Bradley, R. J., & Prasad, K. U. (1983b) *Int. J. Pept. Protein Res. 21*, 16–23.

Veatch, W. R., Fossel, E. T., & Blout, E. R. (1974) *Biochemistry 13*, 5249-5256.
Vega, A. J., & Luz, Z. (1987) *J. Chem. Phys. 86*, 1803-1813.
Venkatachalam, C. M., & Urry, D. W. (1983) *J. Comput. Chem. 4*, 461-469.
Wallace, B. A., Veatch, W. R., & Blout, E. R. (1981) *Biochemistry 20*, 5754-5760.
Weinstein, S., Wallace, B. A., Blout, E. R., Morrow, J. S., & Veatch, W. (1979) *Proc. Natl. Acad. Sci. U.S.A. 76*, 4230-4234.
Weinstein, S., Wallace, B. A., Morrow, J. S., & Veatch, W. R. (1980) *J. Mol. Biol. 143*, 1-19.
Weinstein, S., Durkin, J. T., Veatch, W. R., & Blout, E. R. (1985) *Biochemistry 24*, 4374-4382.

Deuterium NMR of ^{2}HCO-Val^1···Gramicidin A and ^{2}HCO-Val^1-D-Leu^2···Gramicidin A in Oriented DMPC Bilayers†

Andrew W. Hing,*,‡ Steven P. Adams,§ David F. Silbert,∥ and Richard E. Norberg‡

Department of Physics, Washington University, St. Louis, Missouri 63130, Department of Biochemistry and Molecular Biophysics, Washington University, St. Louis, Missouri 63110, and Central Research Laboratory, Monsanto Company, Chesterfield, Missouri 63198

Received June 27, 1989; Revised Manuscript Received December 8, 1989

ABSTRACT: Deuterium NMR is used to study the structure and dynamics of the formyl C–^{2}H bond in selectively deuterated gramicidin molecules. Specifically, the functionally different analogues ^{2}HCO-Val^1···gramicidin A and ^{2}HCO-Val^1-D-Leu^2···gramicidin A are studied by ^{2}H NMR so that any conformational or dynamical differences between the two analogues can be correlated with their difference in lifetime. These analogues are first synthesized, purified, and characterized and then incorporated into oriented bilayers of dimyristoylphosphatidylcholine sandwiched between glass coverslips. Phosphorus NMR line shapes obtained from these samples are consistent with the presence of the bilayer phase and indicate that the disorder exhibited by the lipid matrix is approximately of the same type and degree for both analogues. Deuterium NMR line shapes obtained from these samples indicate that the motional axis of the formyl group of gramicidin is parallel to the coverslip normal, that the distribution of motional axis orientations has a width of 7–9°, and that a similar, major conformational and dynamical state exists for the formyl C–^{2}H bond of both analogues. In this state, if the only motion present is fast axial rotation, then the experimentally derived angle between the formyl C–^{2}H bond and the motional axis is consistent with the presence of a right-handed, single-stranded, $\beta^{6.3}$ helical dimer but is not consistent with the presence of a left-handed, single-stranded, $\beta^{6.3}$ helical dimer. However, if fast axial rotation is not the only motion present, then the left-handed, single-stranded, $\beta^{6.3}$ helical dimer cannot be absolutely excluded as a possibility. Also, a second, minor conformational and dynamical state appears to be present in the spectrum of ^{2}HCO-Val^1-D-Leu^2···gramicidin A but is not observed in the spectrum of ^{2}HCO-Val^1···gramicidin A. This minor conformational and dynamical state may reflect the presence of monomers, while the major conformational and dynamical state may reflect the presence of dimers.

One of the most important properties of the linear peptide gramicidin is its ability to form ion channels in model membranes (Hladky & Haydon, 1970, 1972). Ion channels in cell membranes are extremely important for cellular functions such as controlling the internal environment, maintaining a membrane potential, and, in nerve cells, propagating an action potential. It is hoped that the study of a model ion channel such as gramicidin will lead to general insights about how ion channels work. One of the most important insights to be gained is how function is related to structure. Thus, one of the most important questions about gramicidin centers on how the functional aspects of the channel are related to the channel's three-dimensional structure in a membrane.

One of the important functional properties of the gramicidin channel is the channel's kinetics of formation and dissociation. In the process of forming an ion channel, two nonconducting monomers combine to form a conducting dimer (Hladky & Haydon, 1970, 1972; Bamberg & Läuger, 1973, 1974; Zingsheim & Neher, 1974; Kolb et al., 1975; Veatch et al., 1975):

$$G + G \underset{k_D}{\overset{k_R}{\rightleftharpoons}} G_2$$

In this dimerization reaction, k_R is the rate constant of association and k_D is the rate constant of dissociation. The dissociation constant k_D is therefore equal to the reciprocal of the mean lifetime τ^* of a channel (Bamberg & Läuger, 1973; Kolb & Bamberg, 1977):

$$k_D = 1/\tau^* \quad (1)$$

Both rate constants, though, determine the equilibrium con-

†This work was supported in part by NIH Grants GMO7200, GM30244, and GM38540, ACS Grant BC198, the Department of Physics of Washington University, and the Central Research Laboratories of Monsanto Co.

*Address correspondence to this author at the Department of Physics, Box 1105, Washington University, St. Louis, MO 63130.
‡Department of Physics, Washington University.
§Monsanto Co.
∥Department of Biochemistry and Molecular Biophysics, Washington University.

0006-2960/90/0429-4156$02.50/0